Received: 20 February 2021 | Revised: 11 August 2021 | Accepted: 9 September 2021

DOI: 10.1111/jnc.15517

Journal of Neurochemistry JNC The Official Journal of the International Society for Neurochemistry WILEY

ORIGINAL ARTICLE

EFhd2 brain interactome reveals its association with different cellular and molecular processes

Ahlam S. Soliman[1,2,3] | Andrew Umstead[1,4] | Tessa Grabinski[1] | Nicholas M. Kanaan[1,2,5] | Andy Lee[6] | John Ryan[6] | Jared Lamp[1,4] | Irving E. Vega[1,2,4,5,7]

[1]Department of Translational Neuroscience, College of Human Medicine, Michigan State University, Grand Rapids, Michigan, USA

[2]Neuroscience Program, Michigan State University, Grand Rapids, Michigan, USA

[3]Department of Clinical Pharmacy and Pharmacy Practice, Faculty of Pharmacy, Cairo University, Cairo, Egypt

[4]Integrated Mass Spectrometry Unit, College of Human Medicine, Grand Rapids, Michigan, USA

[5]Hauenstein Neuroscience Center, Mercy Health Saint Mary's, Grand Rapids, Michigan, USA

[6]NeuroInitiatives LLC, Jacksonville, Florida, USA

[7]Department of Neurology, University of Michigan, Ann Arbor, Michigan, USA

Correspondence
Irving E. Vega, Department of Translational Neuroscience, College of Human Medicine, Michigan State University, 400 Monroe Ave NW, Grand Rapids, MI 49503, USA.
Email: vegaie@msu.edu

Funding information
NIH, Grant/Award Number: P30AG053760

Abstract

EFhd2 is a conserved calcium-binding protein that is highly expressed in the central nervous system. We have shown that EFhd2 interacts with tau protein, a key pathological hallmark in Alzheimer's disease and related dementias. However, EFhd2's physiological and pathological functions in the brain are still poorly understood. To gain insights into its physiological function, we identified proteins that co-immunoprecipitated with EFhd2 from mouse forebrain and hindbrain, using tandem mass spectrometry (MS). In addition, quantitative mass spectrometry was used to detect protein abundance changes due to the deletion of the *Efhd2* gene in mouse forebrain and hindbrain regions. Our data show that mouse EFhd2 is associated with cytoskeleton components, vesicle trafficking modulators, cellular stress response-regulating proteins, and metabolic proteins. Moreover, proteins associated with the cytoskeleton, vesicular transport, calcium signaling, stress response, and metabolic pathways showed differential abundance in Efhd2$^{(-/-)}$ mice. This study presents, for the first time, an EFhd2 brain interactome that it is associated with different cellular and molecular processes. These findings will help prioritize further studies to investigate the mechanisms by which EFhd2 modulates these processes in physiological and pathological conditions of the nervous system.

KEYWORDS
brain, cytoskeleton, EFhd2, mass spectrometry, tauopathies, validation

1 | INTRODUCTION

EF-Hand Domain family member 2 (EFhd2), also known as Swiprosin-1, is a calcium-binding protein that is highly conserved from human to nematodes (Kogias et al., 2019; Vega, 2016). In fact, mouse EFhd2 is 91% identical to the human ortholog (Kogias et al., 2019; Vega, 2016). EFhd2 is a 240-amino acid protein with a polyalanine motif (6–9 alanine) at the N-terminus, which confers its

Abbreviations: AD, Alzheimer's disease; AMBIC, ammonium bicarbonate; ANOVA, analysis of variance; BCR, B cell receptors; CAN, acetonitrile; CBD, corticobasal degeneration; C-C, coiled coil domain; CNS, central nervous system; EFhd2, EF-hand domain family member 2; ELISA, enzyme-linked immunosorbent assay; ER, endoplasmic reticulum; ES, embryonic stem cells; FA, formic acid; FTD, frontotemporal dementia; GO, gene ontology; HCD, high-energy C-trap dissociation; hEFhd2^{WT}, recombinant human EFhd2 wild type; hEFhd2$^{\Delta CC}$, recombinant human EFhd2 truncated at C-terminus; hEFhd2$^{\Delta NT}$, recombinant human EFhd2 truncated at N-terminus; IACUC, institutional animal care and use committee; IP, immunoprecipitation; LFQ, label-free quantification; MS, tandem mass spectrometry; NEM, N-ethylmaleimide; PLCγ, phospholipase C gamma; ppm, parts per million; PRM, parallel reaction monitoring; RBPs, RNA-binding proteins; RF, radio frequency; SLP-65, SH2 domain-containing leukocyte adaptor protein of 65 kDa; SNARE, SNAP receptor; SNP, single-nucleotide polymorphism; Syk, spleen tyrosine kinase; tMS, targeted mass spectrometry; TRiC, T-complex protein 1-Ring complex; UPS, ubiquitin/proteasome system; VTA, ventral tegmental area.

thermostability (Ferrer-Acosta et al., 2013). In addition, EFhd2 has two EF-hand Ca^{2+}-binding domains that span amino acids 95–123 and 131–159. EFhd2 has a dynamic structure with the propensity to self-oligomerize (Ferrer-Acosta, Rodríguez-Cruz, et al., 2013). The coiled-coil domain (C-C) in the C-terminus mediates EFhd2 self-oligomerization (Ferrer-Acosta, Rodríguez-Cruz, et al., 2013). Using proteomic analysis, we reported that EFhd2 is phosphorylated by Cdk5 at Ser74. Interestingly, phosphorylated EFhd2 showed low Ca^{2+}-binding activity (Vazquez-Rosa et al., 2014).

EFhd2 is widely expressed in most organs with predominant levels in the central nervous system (CNS) (Vega et al., 2008). In particular, it is abundant in forebrain regions such as the hippocampus, frontal cortex, and olfactory bulb with lower levels in the cerebellum and brain stem (Purohit et al., 2014). Reportedly, EFhd2 is mainly expressed in the grey matter where it localizes to the somatodendritic synaptic compartments (Borger et al., 2014; Ferrer-Acosta, Rodríguez-Cruz, et al., 2013; Purohit et al., 2014). However, the biological role of EFhd2 is still unclear. Previous studies suggested that EFhd2 is involved with different signaling pathways in immune cells (Kogias et al., 2019). For instance, in B cells, EFhd2 inhibits B-cell receptor (BCR)-induced NF-κB signaling, which then downregulates antiapoptotic protein BCL-XL (Avramidou et al., 2007). Moreover, EFhd2 enhances BCR-induced Ca^{2+} influx by acting as a scaffold protein for Syk, SLP-65, and PLCγ (Kroczek et al., 2010). Collectively, these data suggest a role of EFhd2 in B cells survival or lifespan. In T cells, EFhd2 is abundant in microvilli-like membrane structures and lamellipodia where it associates with F-actin structures (Kwon et al., 2013). Further characterization of EFhd2 showed that it mediates cell spreading and migration, possibly, by regulating actin bundling and polymerization (Kwon et al., 2013). However, it is still unknown how EFhd2 modulates actin structures and mediates cell migration.

EFhd2 has been associated with cancer and neurodegeneration. Consistent with its role in modulating cell migration and survival, EFhd2 is highly expressed in a multitude of invasive human cancers (Huh et al., 2015). Ectopic overexpression of EFhd2 led to pulmonary metastasis by activating Rho family of GTPases. Therefore, EFhd2 is associated with cancer invasion and represents a potential therapeutic target (Huh et al., 2015; Peled et al., 2018). In the CNS, we provided evidence that EFhd2 is associated with tauopathies (Vega et al., 2008). Tauopathies are a heterogeneous group of neurodegenerative diseases that encompass Alzheimer's disease (AD), frontal temporal dementias (FTDs), corticobasal degeneration (CBD), among others (Dujardin et al., 2018). The cardinal pathological hallmark in all tauopathies is the aberrant aggregation of microtubule-associated protein tau. During the disease trajectory, tau undergoes conformational changes and transitions from soluble monomers to oligomeric structure to ultimately insoluble paired helical filaments leading to neurodegeneration (Dujardin et al., 2018; Götz et al., 2019). The molecular mechanisms that underlie abnormal tau depositions are unknown. We showed that EFhd2 copurified with pathological tau in a mouse model of tauopathy and postmortem AD human brains (Ferrer-Acosta, Rodríguez-Cruz, et al., 2013; Vega et al., 2008). EFhd2 interacts with the microtubule domain of tau to induce the formation of amyloid structure in vitro (Vega et al., 2018). Moreover, EFhd2 transforms the liquid phase behavior of tau into solid-like structures (Vega et al., 2019). Taken together, these findings highlight the potential role of EFhd2 in modulating tau aggregation. However, further studies are required to delineate the mechanism by which EFhd2 contributes to tau-mediated neurodegeneration (reviewed in Vega, 2016).

To gain insights into EFhd2's biological function, we generated an Efhd2 knockout mouse model ($Efhd2^{(-/-)}$) (Rodriguez-Cruz, 2014). $Efhd2^{(-/-)}$ mice develop without gross anatomical, developmental, or morphological anomalies, despite impaired dendritic morphology in the CNS (Purohit et al., 2014; Regensburger et al., 2018; Rodriguez-Cruz, 2014). Other studies suggested that EFhd2 proteins regulate the behavioral response to alcohol and drug addiction (Kogias et al., 2019). $Efhd2^{(-/-)}$ mice show increased alcohol consumption (Mielenz et al., 2018) and behavioral changes to psychostimulant drugs invoked by enhanced monoaminergic response in the reward system (Kogias et al., 2020). Moreover, it was demonstrated that EFhd2 impedes kinesin-mediated axonal transport in cultured hippocampal neurons (Purohit et al., 2014). These data indicate that EFhd2 may promote resilience against addiction and play a potential role in neuronal transport and survival. At present, however, the molecular mechanisms by which EFhd2 modulates resilience and neuronal survival have yet to be investigated.

Despite the strides other colleagues and we have made to unveil EFhd2's function in the brain, its biological function remains poorly understood. To broaden our understanding of EFhd2's function in the brain, we sought to identify EFhd2-associated proteins in adult mouse brain. EFhd2 was immunoprecipitated from forebrain (i.e., cerebrum including limbic system, basal ganglia, and diencephalon) and hindbrain (i.e., cerebellum and brainstem) regions of EFhd2 wild type ($Efhd2^{(+/+)}$) mice. The associated proteins were identified by tandem mass spectrometry (MS) (Figure 1a). Additionally, to uncover molecular pathways associated with EFhd2 function, label-free quantitative (LFQ) proteomics was used to identify proteome changes in forebrain and hindbrain regions due to the deletion of the *Efhd2* gene ($EFhd2^{(-/-)}$) (Figure 1a). Herein, the data indicate that EFhd2 in mice forebrain and hindbrain regions are associated with cytoskeleton components, vesicle trafficking modulators, cellular stress response-regulating proteins, and metabolic proteins. Moreover, *Efhd2* deletion affected the abundance of proteins associated with metabolic pathways, transport, stress response and protein localization in forebrain and hindbrain regions. These findings serve as a foundation for further studies directed to uncover the role of EFhd2 in different physiological and pathological pathways.

2 | MATERIALS AND METHODS

This study was not pre-registered

2.1 | Reagents

VWR International (Radnor, Pennsylvania): AMBIC (cat. no. BDH9206), Tris (AMRESCO, cat. no. 0497). Thermo Fisher

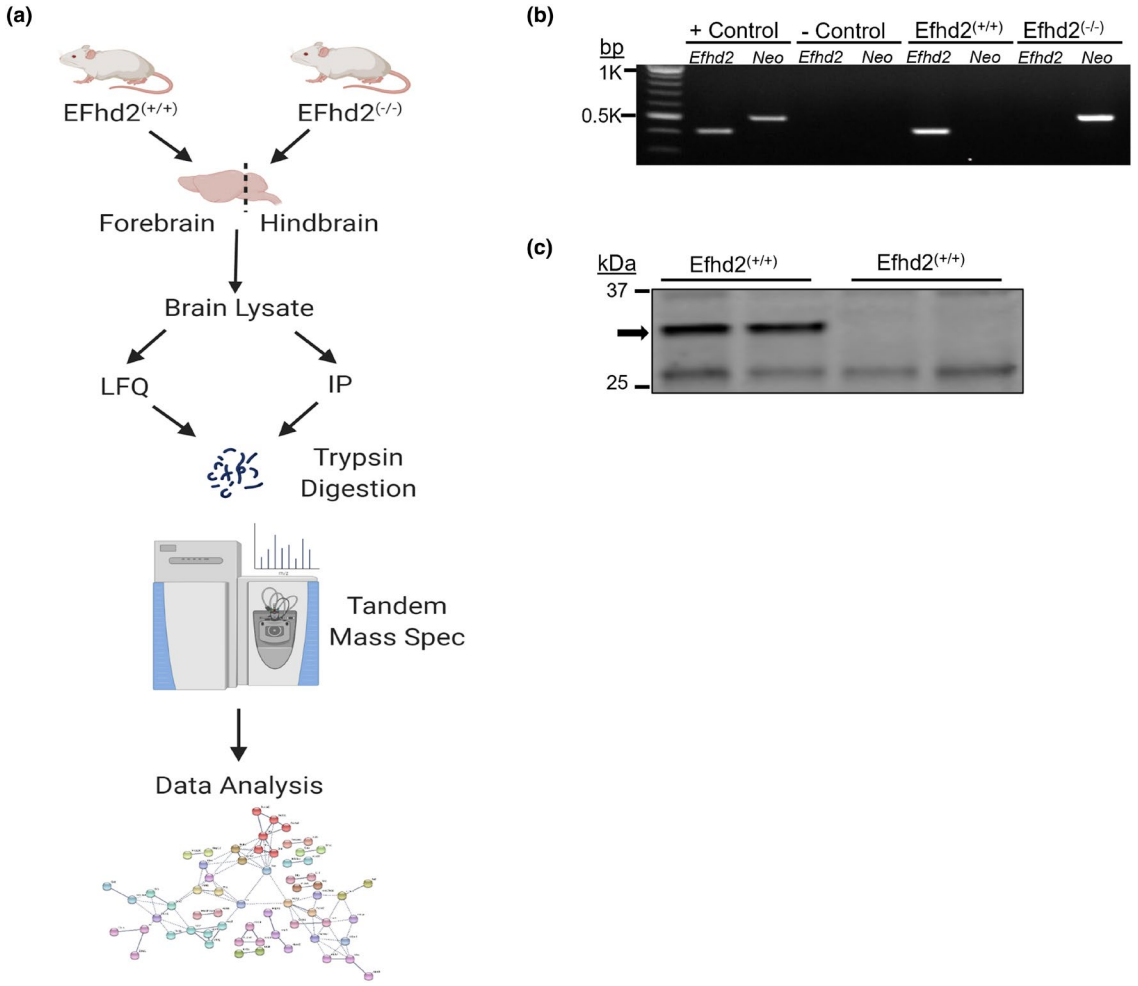

FIGURE 1 Experimental design. (a) Workflow for identifying EFhd2-associated proteins in mouse brain tissues and proteome changes in Efhd2$^{(-/-)}$ (created in BioRender.com) (b) PCR-based genotyping. It shows the presence of Efhd2 in the wild type (Efhd2$^{(+/+)}$) while detection of the Neomycin cassette (*Neo*) verifies the knockout (Efhd2$^{(-/-)}$). DNA base pair (bp) ladder was used. (c) Western blot using anti-EFhd2 (clone 10D6) antibody for 45 μg of postnuclear brain lysates of Efhd2$^{(+/+)}$ and Efhd2$^{(-/-)}$. The arrow indicates EFhd2 protein band. Molecular weight markers (kDa) are indicated

scientific: Acetonitrile (Fisher Scientific, cat. no. A955-4), EDTA (Acros Organics, cat. no. 60-00-4), EGTA (Acros Organics, cat. no. 67-42-5), NaF (Acros Organics, cat. no. 7681-49-4), Sodium Pyrophosphate (Alfa Aesar, cat. no. 13472-36-1). MilliporeSigma: Formic Acid (cat. no. F0507).

2.2 | Commercial antibodies

Antibodies were selected to validate selected EFhd2-associated proteins by western blot. Western blot analysis was performed to verify the specificity of commercial antibodies using whole-brain extracts (data not shown). We used antibodies that detected a protein band at the expected molecular weight of the targeted protein. Thermo Fisher scientific: Rabbit polyclonal anti-transgelin 3 (cat. no. 12246-1-AP,1:250); Rabbit monoclonal anti-tropomodulin 2 (cat. no. MA5-36150, 1:250); Rabbit polyclonal anti-coronin 2b (cat. no. 13802-1-AP,1:250). Cell Signaling Technology (Danvers, Massachusetts): Rabbit polyclonal anti-myosin 2a (cat. no. 3403, 1:500), Rabbit monoclonal anti-myosin 2b (cat. no. 8824, 1:500).

2.3 | Monoclonal Anti-EFhd2 antibody production

A mouse monoclonal anti-EFhd2 (clone 10D6) antibody was generated in Efhd2$^{(-/-)}$ mice using methods similar to those previously described (Grabinski & Kanaan, 2016). Briefly, animals received subcutaneous injections of hEFhd2$^{\Delta CC}$ protein (100 μg protein in adjuvant) every 3 weeks until sufficient titers were achieved (signal above-background at ≥1:2,621,440 dilution). Hybridoma fusion techniques (Binder et al., 1985; Grabinski & Kanaan, 2016) were used, and cultures were screened for reactivity against the hEFhd2$^{\Delta CC}$, hEFhd2$^{\Delta NT}$, and hEFhd2^{WT} protein by indirect enzyme-linked immunosorbent assay (ELISA, see below). Positive clones were subcloned at least three times as described (Grabinski & Kanaan, 2016). Antibody isotype was determined using the IsoStrip Mouse

Monoclonal Antibody Isotyping Kit (Roche, cat. no. 11493027001), and mycoplasma testing was performed using the Mycoplasma PCR ELISA kit (Roche, cat. no. 11663925910). After the clone was verified as clean, stable, and positive, the line was grown in a CELLine 350 bioreactor (Integra Biosciences), and the antibody was purified by Protein A affinity chromatography (GE Healthcare, cat. no. 17-1279-01) and stored at 1 mg/ml in 10 mM HEPES, 500 mM NaCl, 50% Glycerol. This new anti-EFhd2 antibody will be shared upon reasonable request.

2.4 | Anti-EFhd2 antibody validation

ELISAs were performed to determine the binding affinity and specificity of the EFhd2 antibody for EFhd2 protein using previously detailed methods (Grabinski & Kanaan, 2016). Briefly, hEFhd2$^{\Delta CC}$, hEFhd2$^{\Delta NT}$, and hEFhd2^{WT} (50 µl at 2 ng/µl in borate saline) coated onto wells of a 96-well plate (Corning, cat. no. 3590) for 1h. Wells were washed (wash solution: 100 mM boric acid, 25 mM sodium tetraborate decahydrate, 75 mM NaCl, 250 µM thimerosal, 0.4% bovine serum albumin and 0.1% Tween 20), blocked in blocking buffer (5% non-fat dry in wash solution; 200 µl/well) for 1 h, and then incubated in purified anti-EFhd2 clone 10D6 antibody (1 mg/ml stock; serially diluted from 1:100 to 1:17,714,700 – in blocking buffer; 2 h). Wells were washed and incubated in goat anti-mouse HRP conjugated antibody (1:5,000; Jackson ImmunoResearch, cat. no. 15-035-003; 1 h). Wells were washed, and then reactivity was detected with 3,3′,5,5′ tetramethylbenzidine substrate (50 µl/well; Sigma, cat. no. T0440; 8 min development). Reactions were quenched with 50 µl 3.6% H_2SO_4, and then the absorbance was read at 450 nm. All washes were done 3 times with 200 µl/well of wash solution, and antibodies were diluted in blocking buffer. Blank wells were used to obtain background absorbance, which was removed from sample signals. Absorbance values were converted to percent light absorbed and data analyzed using sigmoidal non-linear curve fitting to obtain titer values (Figure S2).

2.5 | Animals

All animals use protocol was approved by Michigan State University's Institutional Animal Care and Use Committee (IACUC protocol #04-18-052-00). Efhd2$^{(-/-)}$ was generated from targeted embryonic stem (ES) cells for EFhd2 obtained from the KOMP Repository (www.komp.org), an NCRR-NIH supported mouse strain repository (U42-RR024244). The ES cells (C57BL/6N-Efhd2 $^{rm1(KOMP)Vlcg}$) were created by Velocigene (Valenzuela et al., 2003). *Efhd2* gene knockout in ES cells was performed by homologous recombination using a targeting vector (Neo-LacZ) (KOMP Repository, UC Davies (Pettitt et al., 2009). ES cells were electroporated with a neomycin (G418)-Lac Z clones. A 60% euploid clone was injected into C57BL/6 mouse blastocysts, from which chimeric males were obtained. Chimeras were bred with C57BL/6 wild-type females. After establishing Efhd2$^{(-/-)}$ colony in the C57BL/6, females and males were crossed with Swiss Webster mice, and the genomic background was assessed. To assess genomic background, we used the genomic marker developed by DartMouse™. This strategy utilizes single-nucleotide polymorphisms (SNP) spread throughout the genome to determine the contribution of genomic DNA when different mouse strains are crossed, providing greater efficiency towards reaching a homogenous genomic background colony. Starting F2, we generated the three main genotypes, namely Efhd2$^{(+/+)}$, Efhd2$^{(+/-)}$ and Efhd2$^{(-/-)}$. Based on genomic markers data, from generation F4 forward, the mouse colony shows a stable mixed SW/C57BL/6 genomic background (Figure S1). In this study, age-matched (11–12 months) female Efhd2$^{(+/+)}$ and Efhd2$^{(-/-)}$ mice were used. Males were excluded from the study. The selected age and sex were based on previous studies that indicated higher EFhd2 abundance in adult mice regardless of sex (Purohit et al., 2014; Rodriguez-Cruz, 2014). In addition, Female Efhd2$^{(-/-)}$ at this age do not show behavior or motor impairment compared to their wild type littermates (Purohit et al., 2014; Rodriguez-Cruz, 2014). Their activity level is comparable to age-matched wild type. Mice were socially housed (up to 5 mice per cage), and food and water were provided ad libitum. Mice were transferred to a clean cage with food and water weekly. No sample calculation was performed. Sample size was determined according to previous studies that indicated the minimum number of samples to achieve a power of 0.90 (Levin, 2011). Six mice per group were used for global proteome discovery of EFhd2-associated proteins and LFQ. Three mice per group were used for the subsequent validation of EFhd2-associated proteins by western blot and targeted mass spectrometry (tMS). Inclusion criteria were defined by genotype and sex. Simple randomization was used to select mice per genotype. Animals were euthanized by CO_2 suffocation, and tissues were extracted as described previously (Vega et al., 2008).

2.6 | Genotyping

Genotyping was performed by extracting DNA from ear punches at weaning (21 days) using Kappa Mouse Genotyping Kit (GE cat. no. KK7352) according to manufacturers' recommendations (Figure 1b). Amplification of the LacZ gene was performed using the *3' Uni Neo* (5'GCAGCCTCTGTTCCACATACACTTCA3') and *Reg 10032R1 (5' GCCTATAGTTAAGGGGAGTTGGGTGG 3')* primers. For the *Efhd2* gene, *Efhd2 Fwd* (5' CTTGGCCTCGAAGAAGTTCTTGG3') and *Efhd2 Rev* (5'GCCCTCTAAGGCTTTGTGAATGC3') primers were used. Amplification of both genes was performed using cycling conditions recommended by the KOMP consortium. PCR reaction: 12.5 µl 2x Kappa Fast genotyping, 1.25 µl Primer Fwd (100 ng/µl), 1.25 µl primer Rev (100 ng/µl), 1 µl extracted DNA and 9 µl ddH_20. Western blot was used to confirm the genotyping results (Figure 1c).

2.7 | Tissue processing

The experimental design is illustrated in Figure 1a. Efhd2$^{(+/+)}$ ($n = 6$) and Efhd2$^{(-/-)}$ ($n = 6$) forebrain (i.e., cerebrum including limbic system, basal ganglia, and diencephalon) and hindbrain (i.e., cerebellum and brainstem) regions were homogenized in five volumes of 20 mM Tris Base, pH 7.4, 150 mM NaCl, 1 mM EDTA, 1 mM EGTA, 5 mM sodium pyrophosphate, 30 mM NaF, and supplemented with 1X Halt protease inhibitor cocktail (Thermo Scientific, cat. no. 78430). Brain homogenate was centrifuged at 18,400 *g*, 4°C for 10 min, and the supernatant (postnuclear lysate) was transferred to a clean tube to estimate its protein concentrations using BCA Assay (Pierce, cat. no. 23225). The same tissue protein lysates were used for identification of EFhd2-associated proteins (immunoprecipitation-MS) and LFQ. MS samples processing and tissue processing were conducted by different personnel.

2.8 | Identification of EFhd2-associated proteins

2.8.1 | Immunoprecipitation (IP)

Postnuclear lysates were incubated with Protein A/G-conjugated magnetic beads (Pierce, cat. no. 88803) for 3 h at 4°C with constant rotation. This step is crucial to preclear samples from endogenous immunoglobulins and other proteins that nonspecifically bind to the beads. Afterwards, sample tubes were placed on a magnetic strip, and the supernatant (precleared lysate) was transferred to clean tubes. BCA assay was performed to estimate the precleared lysate protein concentration. Three micrograms of anti-EFhd2 (clone 10D6) were added to 2 mg of precleared lysate and incubated with constant rotation for 17 h at 4°C. Then, Protein A/G-conjugated magnetic beads were added and incubated at 4°C for 4 h. The supernatant was transferred to clean tubes and the beads were washed 4 times with 25 mM ammonium bicarbonate (AMBIC), pH 8. After the final wash, beads were split evenly for western blot and MS.

2.8.2 | Western blot

After washing the beads, the wash buffer was completely removed, and beads were resuspended in SDS-loading buffer containing N-ethylmaleimide (2X NEM) instead of β-mercaptoethanol and incubated overnight at 4°C. Mouse immunoprecipitates along with 45 μg of the respective postnuclear lysates (input) were resolved on 4–20% SDS-PAGE gels and transferred to nitrocellulose membranes (0.45 μm, BIO-RAD, cat. no. 1620115). The membranes were blocked by 5% non-fat dry milk in 1X TBST (2.5 mM Tris-Base, 15 mM NaCl, 30 mM KCL, 0.1% Tween 20) for 1 h at room temperature (24°C). Then, the membranes were incubated in 1:5000 Anti-EFhd2 (clone 10D6) overnight at 4°C. After primary incubation, membranes were washed three times in 1X TBST and then incubated in 1:2000 of appropriate secondary antibody (LI-COR) at 24°C for 1 h. Subsequently, membranes were washed three times in 1X TBST. Membranes were visualized by the LI-COR Odyssey Imaging System and analyzed using Image Studio (v5.2).

2.8.3 | Protein digestion

After IP, beads were resuspended in the digestion buffer (25 mM AMBIC/50% acetonitrile (ACN)), and rLys-C (500 ng Promega, cat. no. V1671) were added to each sample and incubated at 37°C for 1.5 h. Afterwards, 1 μg trypsin (Promega, cat. no. V5280) was added to the samples and incubated at 37°C for 17 h. The digestion solution was transferred to clean tubes and dried completely using a speed vacuum at 30°C. Finally, samples were resuspended in 50 μl of 25 mM AMBIC/5% ACN.

2.8.4 | Liquid chromatography tandem mass spectrometry

nanoLC-MS/MS separations were performed with a Thermo Scientific™ Ultimate™ 3000 RSLCnano System. Peptides were desalted in-line using a C18 trap cartridge (300 μm × 5 mm) with 2% ACN, 0.1% formic acid (FA) for 5 min with a flow rate of 5 μl/min at 40°C. The trap cartridge was then brought in-line with a 2 μm diameter bead, C18 EASY-Spray™ column (75 μm × 250 mm) for analytical separation over 120 min with a flow rate of 350 nl/min at 40°C. The mobile phase consisted of 0.1% FA (buffer A) and 0.1% FA in ACN (buffer B). The separation gradient was as follows: 5 min desalting, 95 min 4–40% B, 2 min 40–65% B, 3 min 65–95% B, 11 min 95% B, 1 min 95–4% B, 3 min 4% B. Three microliters of each sample were injected.

Top 20 data-dependent mass spectrometric analysis was performed with a Q Exactive™ HF-X Hybrid Quadrupole-Orbitrap™ Mass Spectrometer. MS1 resolution was 60K at 200 m/z with a maximum injection time of 45 ms, AGC target of 3e6, and scan range of 300–1500 m/z. MS2 resolution was 60K at 200 m/z, with a maximum injection time of 118 ms, AGC target of 5e3, and isolation range of 1.3 m/z. HCD normalized collision energy was 28. Only ions with charge states from +2 to +6 were selected for fragmentation, and dynamic exclusion was set to 30 s. The electrospray voltage was 1.9 kV at a 2.0 mm tip to inlet distance. The ion capillary temperature was 280°C and the RF level was 55.0. All other parameters were set as default.

2.8.5 | Protein identification

Protein identification was conducted by Proteome Discoverer™ Software version 2.2.0.388. Spectra were searched with Sequest HT against the Mus musculus Uniprot protein database (61204 unique sequences). Enzyme specificity was set to trypsin with an MS1 tolerance of 10 ppm and a fragment tolerance of 0.02 Da. Oxidation (M), acetylation (protein N-term), and methionine loss (protein N-term)

were set as dynamic modifications. False discovery rates were set to 0.01 using the Percolator node. Two unique peptides were required for protein identification. All other parameters were set as default. The data was curated to correct discrepancies in the accession number and deleting all proteins that were also identified in the negative control (IP from Efhd2$^{(-/-)}$ brain regions).

2.8.6 | Validation of EFhd2-associated proteins

The proteins selected for validation needed to fulfil the following criteria: (1) detection in both forebrain and hindbrain regions of mouse brain (2) involved in specific molecular processes to which EFhd2 was previously associated, and (3) availability and validation of commercial antibodies. Forebrain and hindbrain from Efhd2$^{(+/+)}$ ($n = 3$) and Efhd2$^{(-/-)}$ ($n = 3$) mice were used to validate the EFhd2-associated proteins identified by MS. To take in consideration biological variability, the three tissue samples for each region were pooled and homogenized. Thus, we generated one tissue lysate from the mice forebrains and hindbrains. IP and western blot were performed as explained above. In addition, a targeted mass spectrometry (tMS) approach was developed to account for differences in sensitivity between western blot and MS analyses. Target peptides were selected from the peptides identified in the data-dependent mass spectrometry experiments (see *Liquid Chromatography Tandem Mass Spectrometry* section). tMS chromatography was identical to the chromatography described above, except for the following changes. tMS peptides were separated using a C18 trap column (75 μm × 20 mm) in-line with a 3 μm diameter bead, C18 EASY-Spray™ separation column (75 μm × 150 mm) for analytical separation over 130 min. The separation gradient was as follows: 100 min 4–40% B, 2 min 40–65% B, 3 min 65–95% B, 11 min 95% B, 1 min 95–4% B, 13 min 4% B. One microliter of each sample was injected.

Skyline v 4.2 was used to configure peptide isolation lists for parallel reaction monitoring (PRM). Targeted scans were collected using an unscheduled inclusion list. Fragment ion spectra were acquired at 60K at 200 m/z, with a maximum injection time of 100 ms, and AGC target of 2e5. All other parameters were as described above. Skyline was also used to evaluate PRM data. Peptide retention times were manually refined. MS/MS mass tolerance filtering matched the acquisition method (60K at 200 m/z). The top 3 fragment ions as ranked by Skyline were compared to the NIST Mouse HCD Library (maximum library rank of 6) to validate the detected product ions against an established database (CHEMDATA.NIST.GOV 2021). Peptide dot products and peak areas were calculated by Skyline. Dot products under 0.7 were not considered a positive identification of the product ions.

2.8.7 | Label-free quantification (LFQ)

Three 10 μg aliquots of postnuclear lysate from Efhd2$^{(+/+)}$ ($n = 6$) and Efhd2$^{(-/-)}$ ($n = 6$)) forebrain and hindbrain were buffer exchanged 4 times into 500 μl 25 mM AMBIC, pH 8.0 using an Amicon ultra 3 kDa centrifugal filter (Millipore, cat. no. UFC-500396). Samples were centrifuged at 18,400 *g*, 4°C for 10 min per exchange. After exchanging, samples were dried completely using a speed vacuum at 30°C and stored at −20°C before digestion. Samples were digested in sets of nine, each sample consisting of three technical replicates. Samples were resuspended in 50 μl 25 mM AMBIC in 50% ACN containing 500 ng rLys-C (Promega, cat. no. V1671), and incubated at 37°C for 1.5 h. Then, 1 μg trypsin (Promega, cat. no. V5280) was added to each sample and incubated at 37°C for 17 h. After digestion, samples were dried completely before resuspension in 50 μl 25 mM AMBIC in 5% ACN. Liquid Chromatography Tandem Mass Spectrometry was performed over 120 min using a 2 μm diameter bead, C18 EASY-Spray™ column (75 μm × 250 mm). The separation gradient was as follows: 5 min desalting, 40 min 4–40% B, 2 min 40–65% B, 2 min 65–95% B, 7 min 95% B, 1 min 95–4% B, 3 min 4% B. Protein identification proceeded as previously described for the IP samples. Quantitative ratios were determined using the Precursor Ion Quantitation node. This node calculates the abundance of a peptide as the summation of its quantitative peptide spectral matches. Peptide ratios are determined in a pairwise manner from the geometric median of all combinations of peptide abundance ratios. Protein ratios are determined from the geometric median of all combinations of peptide ratios. *P*-values were determined by ANOVA (background based) and adjusted for multiple comparisons with the Benjamini-Hochberg procedure. Due to missing values in LFQ, we curated the protein list retaining quantitated proteins with, at least, 80% of normalized values in one experimental group (i.e., EFhd2$^{(+/+)}$ or EFhd2$^{(-/-)}$). Data were not assessed for normality and no test for outliers was conducted. The figure was generated using GraphPad Prism 8.

2.8.8 | Gene ontology (GO) enrichment analysis

Cytoscape (v3.8.0) and the ClueGO application (v2.5.7) with the following selection criteria: Statistical Test Used = Enrichment/Depletion (Two-sided hypergeometric test), Correction Method Used = Benjamini-Hochberg, Min GO Level = 1, Max GO Level = 4, Cluster #1, Number of Genes = 10, Min Percentage = 5.0, GO Fusion = false, GO Group = true, Kappa Score Threshold = 0.5, Group By Kappa Statistics = true, Initial Group Size = 1, Sharing Group Percentage = 50.0, Organism analyzed: Mus Musculus [10090], Identifier types used: [AccessionID, UniProtKB_AC], Evidence codes used: [All_without_IEA]. Figures were created using BioRender.com.

3 | RESULTS

3.1 | EFhd2 interactome in mouse brain

EFhd2's physiological and molecular functions are not yet completely understood. Identification of EFhd2's interactome will unravel its association with specific cellular processes, especially in

the brain where it is highly abundant. EFhd2 was immunoprecipitated from forebrain and hindbrain brain regions of Efhd2$^{(+/+)}$ using a novel anti-EFhd2 antibody (Figure S2). Efhd2$^{(-/-)}$ mice were included as a negative control to detect non-specific–binding proteins. Immunoprecipitation (IP) of EFhd2 from the forebrain region was confirmed using western blot (Figure 2a, lanes 1–6). As expected, no EFhd2 bands were observed in IP samples from Efhd2$^{(-/-)}$ forebrain samples (Figure 2a, lanes 7–12). Likewise, EFhd2 was immunoprecipitated from hindbrain regions of Efhd2$^{(+/+)}$ (Figure 2b lanes 1–6), but not from Efhd2$^{(-/-)}$, as expected (Figure 2b lanes 7–12).

Proteins that copurified with EFhd2 were identified by MS. Data were curated by excluding proteins detected in both Efhd2$^{(-/-)}$ and Efhd2$^{(+/+)}$ IPs (see Methods). After data curation, 53 and 73 proteins were identified co-immunoprecipitating with EFhd2 in forebrain and hindbrain regions, respectively. Fourteen EFhd2-associated proteins were identified in both regions (Myh9, Myh10, Myl12b, Myl6, Myo5a, Tmod2, Coro2b, Tagln3, Capza2, Capzb, Sptbn2, Dnm1, Rpl13, EWRS1). To determine the represented biological functions among the identified EFhd2-associated proteins, we conducted a literature search using keywords "*protein name* and brain" or "*protein name* and neuron." The functional categories represented in Figure 3 include at least two proteins per group. Therefore, categories with only one protein are not represented here nor are the proteins of unidentified or not fully investigated biological relevance. However, all proteins are listed in Tables S1 and S2.

3.1.1 | EFhd2 interactome in the forebrain

EFhd2-associated proteins in forebrain are illustrated in Figure 3a. EFhd2 was associated with acting-binding proteins known to regulate actin cytoskeleton dynamics (e.g., Cfl1, Capza2, Dbn1, and Tmod2). Moreover, the data showed that EFhd2 associates with actin-crosslinking proteins like Sptbn1, Sptbn2, Add1, and Ank2. Actin-binding (Myh9, Myh10, Myo5a) and microtubule-binding (Kif5b) motor proteins also co-immunoprecipitated with EFhd2. In addition to actin-binding proteins, intermediate filament proteins in neurons and astrocytes co-immunoprecipitated with EFhd2 (Gfap, Nefh, Nefl, and Nefm). Several proteins that regulate membrane trafficking and cellular transport were also identified (Figure 3a). For example, SNARE complex proteins (Vamp2, Snap25, and Stx1b) control synaptic vesicle docking and fusion (Brunger et al., 2009; Jahn & Fasshauer, 2012; Südhof & Rothman, 2009). Synaptotagmin-like protein Sytl4, its interactor Rab8a, and Dnm1 (involved in clathrin-dependent endocytosis) were also identified as EFhd2-associated proteins, suggesting that EFhd2 associates with known protein complex that mediate vesicle trafficking. Based on these results, EFhd2 is associated with proteins involved in cytoskeletal reorganization, vesicle trafficking, and cellular transport likely in both neurons and astrocytes.

The data analysis also revealed the association of EFhd2 with signaling and stress response proteins. Among the identified proteins, Camk2a and Camk2b are α and β isoforms of CamKII (Gaertner et al., 2004). Map2k1 (MEK1) is an upstream activator of the ERK pathway that regulates cell cycle, survival, and apoptosis (Zhu et al., 2002, 2003). Ogt is responsible for O-GlcNAcylation of proteins that imparts a neuroprotective effect against cellular oxidative stress (Wani et al., 2017). Molecular chaperones of the heat shock proteins family also co-immunoprecipitated with EFhd2. Particularly, Hsp12a and Hsp90aa1 are inducible stress proteins that prevent protein aggregation and enhance cell survival (Wynn et al., 1994). Notably, Hsp12a is an endoplasmic reticulum (ER) stress protein (Kitao et al., 2004). Hsp90aa1 (inducible isoform of Hsp90) mediates nucleus-cytoplasm trafficking of glucocorticoid receptors through interaction with cytoskeletal proteins (Pratt et al., 2006). Taken together, these results suggest that EFhd2 is associated with proteins involved in interrelated molecular pathways that impact neuronal growth, synaptogenesis, and protein homeostasis in forebrain regions.

Along with the cytoskeleton components, trafficking regulators, and stress response proteins, ribosomal proteins (e.g., Rpl13 and Rps15) also copurified with EFhd2. These proteins represent constituents of ribosomes that mediate and control protein synthesis. EFhd2 was associated with several RNA-binding proteins (RBPs) including Sfpq, Nono, and Ewsr1. Ewsr1 is a TET family multifunctional protein that regulates transcription, RNA metabolism and transport, and cellular signal transduction (Lee et al., 2019). Moreover, Nono and Sfpq are components of neuronal RNA transport granules (Kanai

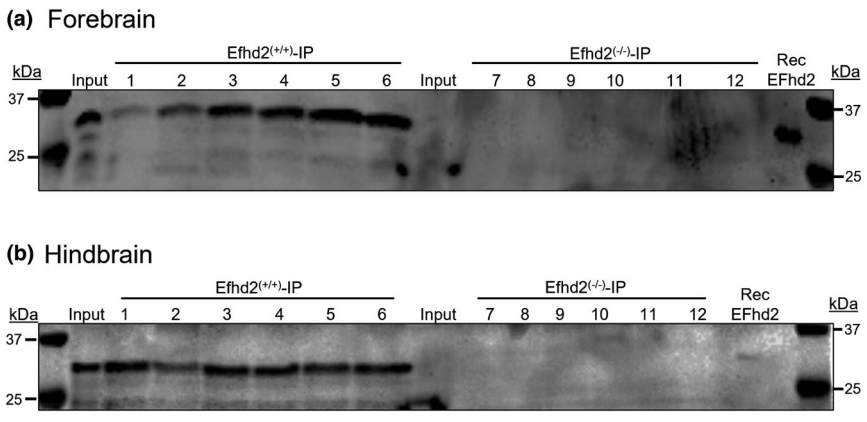

FIGURE 2 EFhd2 immunoprecipitation from forebrain and hindbrain regions of Efhd2$^{(+/+)}$ mice. Western blot using anti-EFhd2 antibody (10D6) confirms EFhd2 IP from Efhd2$^{(+/+)}$ (lanes 1–6, $n = 6$) (a) forebrain and (b) hindbrain regions. No EFhd2 was detected in either input lysates or IP of EFHD2$^{(-/-)}$ (lanes 7–12, $n = 6$). Input is 45 μg postnuclear brain lysate. Recombinant hEFhd2 (5 ng) was used as positive control. (n = number of animals per genotype)

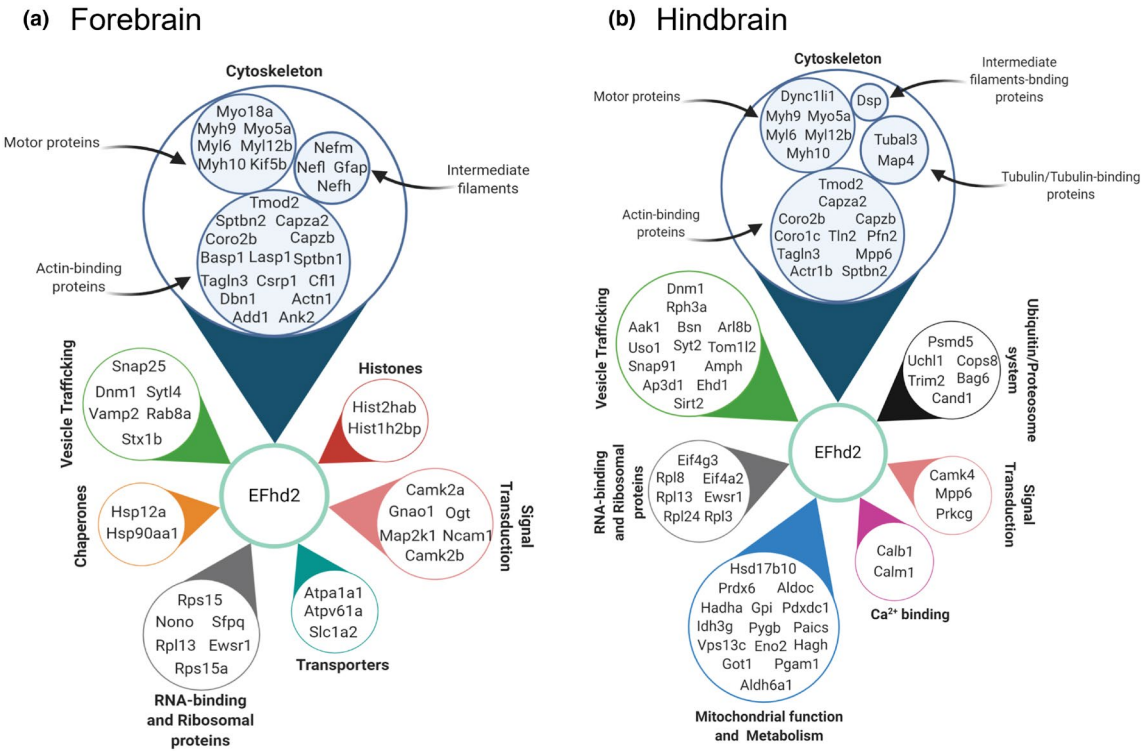

FIGURE 3 EFhd2 brain interactome in mouse brain. EFhd2-associated proteins in the forebrain region (a) and hindbrain (b) of Efhd2$^{(+/+)}$ mice ($n = 6$). EFhd2-associated proteins were categorized according to their known biological function. Only the biological functions that contain two or more proteins are represented. Figure created in Biorender.com. (n = number of animals)

et al., 2004). The transport of RNA granules to axonal ending is indispensable for localized protein synthesis and maintaining RNA and protein homeostasis (Cajigas et al., 2012). It has been shown that Sfpq interacts with Kif5a to regulate RNA granules axonal transport (Fukuda et al., 2021). These findings, together with its association with cell trafficking, indicate that EFhd2 may be involved in the transport of RNA granules and RNA metabolism.

3.1.2 | EFhd2 interactome in the hindbrain

In hindbrain regions, EFhd2 was found in association with proteins involved in biological functions like those identified in the forebrain (Figure 3b). This included actin filaments regulatory proteins such as Pfn2, Sptbn2, Tmod2, and Capza2. In addition, the α-tubulin isoform Tubal3 and microtubule-associated protein Map4 copurified with EFhd2, which suggests an association of EFhd2 with microtubule cytoskeleton dynamics. Furthermore, Dsp is a desmosomal protein that interacts with vimentin to anchor intermediate filaments to the membrane (Meng et al., 1997). Actin- and microtubule-binding motor proteins (Myh9, Myh10, Myl6, and Myo5a) were associated with EFhd2 in both forebrain and hindbrain. Similarly, vesicle trafficking proteins, such as SNARE complex proteins (Snap91) and SNARE interactors (Syt2, Rph3a, and Ehd1) were also found associated with EFhd2 in hindbrain (Ferrer-Orta et al., 2017; Söllner et al., 1993; Wei et al., 2010). Proteins that mediate endocytosis were also identified such as Dnm1, Amph, Tom1l2, and Ap3d1(Cao et al., 1998; Drasbek et al., 2008; Farías et al., 2017; Takei et al., 1999; Wang et al., 2010). These results provide further evidence for the association of EFhd2 with cytoskeleton regulation and trafficking pathways that is consistent in both forebrain and hindbrain.

Hindbrain EFhd2 was associated with cellular homeostasis mechanisms. Specifically, EFhd2 copurified with EF-hand type Ca^{2+}-binding proteins like Calb1 and Calm1 that control calcium homeostasis and impact Ca^{2+}-dependent signaling cascades (Figure 3b). Related to Ca^{2+} homeostasis, EFhd2 was associated with other signaling transduction effectors like Camk4, Mpp6, and Prkcg. Furthermore, Ubiquitin/proteasome system (UPS) components were identified as EFhd2-associated proteins in hindbrain regions (Figure 3b). Proteins with ubiquitin ligase or ubiquitin ligase-regulating activity (e.g., Uchl1, Cand1, and Trim2) co-immunoprecipitated with EFhd2 along with a proteasomal protein Psmd5 (Gong et al., 2016; Khazaei et al., 2011; Pierce et al., 2013). Moreover, Prdx6, a predominantly astrocytic antioxidant enzyme that protects the cell against oxidative stress, was also identified as an EFhd2-associated protein (Power et al., 2008). Consistent with the results from the forebrain, EFhd2 is associated with proteins involved in neuronal growth, stress response, and protein turnover in hindbrain.

In hindbrain regions, EFhd2 was also found associated with proteins that regulate a wide range of metabolic pathways (e.g., Idh3g, Aldh6a1, Hadha, and Aldoc). Additionally, EFhd2 associates with Vps13c and Dnm1l that maintain mitochondrial membrane potential and mitochondrial fission, respectively (Kamerkar et al., 2018; Lesage et al., 2016). In fact, Dnm1l (dynamin-related protein 1 Drp1)

is a large cytosolic GTPase that is recruited to the mitochondrial outer membrane to mediate mitochondrial fission. Thus, EFhd2 is associated with mitochondrial and cytosolic proteins that maintain tight control of metabolism and mitochondrial homeostasis.

3.2 | Global proteome changes upon deletion of *Efhd2*

Mice that lack *Efhd2* develop normally and do not show any phenotype under normal living conditions. However, the absence of the EFhd2 protein may induce proteome changes to compensate for EFhd2's loss of function. To identify proteome changes induced by the deletion of the *Efhd2* gene, we performed global label-free quantitative (LFQ) proteomics analysis in the forebrain and hindbrain regions of Efhd2$^{(-/-)}$ compared to EFhd2$^{(+/+)}$ mice. The data were curated to only assess proteins with abundance changes of at least log2 ± 0.2 (20%) (see Methods). GO enrichment analysis using ClueGo was conducted to investigate which biological functions changed in the absence of the EFhd2 protein. Out of 281 quantified proteins, 123 proteins were grouped into four main biological functions in the forebrain namely metabolism, stress response, protein regulation, and redox. Similarly, GO analysis of the 762 differentially abundant proteins in the hindbrain region categorized 446 proteins into four main biological functions that include metabolism, stress response, protein localization, and transport. (See Tables S3 and S4).

Abundance change of categorized proteins is represented as log2 protein change in Efhd2$^{(-/-)}$ vs Efhd2$^{(+/+)}$ in Figure 4. Most of the forebrain proteins that regulate metabolism showed increased abundance in Efhd2$^{(-/-)}$ (Figure 4a). Likewise, the protein levels of stress response and redox stress response were generally higher in the forebrain regions of Efhd2$^{(-/-)}$. Regarding protein regulation, the number of proteins with increased abundance were almost equal to those with reduced abundance.

Comparable to forebrain LFQ data, most proteins that regulate metabolism in the hindbrain were more abundant in Efhd2$^{(-/-)}$ with respect to Efhd2$^{(+/+)}$ (Figure 4b). Conversely, proteins implicated with protein localization, transport, and stress response showed overall decreased abundance in hindbrain regions of Efhd2$^{(-/-)}$ mice.

Taken together, *Efhd2* gene deletion induces changes in proteins that mediate different cellular processes including metabolism, redox, stress response, protein transport, and trafficking. These processes are overrepresented among the identified EFhd2-associated proteins, which led us to examine which novel identified EFhd2-associated proteins also change upon deletion of the Efhd2 gene. Figure 5 shows identified EFhd2-associated proteins in forebrain and hindbrain regions (green nodes indicate increased abundance and red nodes indicate decreased abundance). Eleven proteins differentially abundant in Efhd2$^{(-/-)}$ compared to Efhd2$^{(+/+)}$ were associated with EFhd2 in both forebrain and hindbrain regions (Figure 5a,b). These proteins include cytoskeletal proteins (Capzb, Coro2b, Myh10, Myh9, Myl12b, Myl6, Sptbn2, and Tmod2), membrane trafficking protein (Dnm1), and RBPs and Ribosomal proteins (Ewsr1 and Rpl13). In addition, 6 unique forebrain EFhd2-associated proteins showed more than log2 ±0.2 change (Figure 5a and Table S7). Primarily, they are cytoskeletal proteins and RBPs. In the hindbrain, we found that 24 unique EFhd2-associated proteins had more than log2 ±0.2 abundance change (Figure 5b). These proteins are involved in cytoskeleton dynamics, vesicle trafficking, metabolism, RNA-binding, signal transduction, and UPS (Figure 5b and Table S8). The convergence of LFQ and EFhd2 interactome data establish an intrinsic relationship between EFhd2 and these specific biological processes.

3.3 | Validation of selected EFhd2-associated proteins

To confirm the identified EFhd2-associated proteins, we selected 5 proteins for validation by western blot. These proteins were chosen based on (1) detection in both forebrain and hindbrain regions of mouse brain, (2) association with molecular processes to which EFhd2 has been previously linked, and (3) availability and validation of commercial antibodies. The selected proteins include transgelin-3 (Tagln3), tropomodulin 2 (Tmod2), and coronin 2b (Coro2b), which are known to regulate actin dynamics and organization. In addition, myosin 2a (Myh9) and myosin 2b (Myh10) are non-muscle myosin II heavy chain isoforms. Non-muscle myosin II is an actin-binding motor protein that regulates cross-linking and bears contractile properties (Vicente-Manzanares et al., 2009). EFhd2 was immunoprecipitated from forebrain and hindbrain of Efhd2$^{(+/+)}$ (n = 3). Efhd2$^{(-/-)}$ (n = 3) were again used as a negative control to ensure that the selected proteins do not bind nonspecifically to either the beads or the antibody. The co-immunoprecipitation of EFhd2 with the five selected proteins was detected by western blot (Figure 6). Total lysate from Efhd2$^{(+/+)}$ and Efhd2$^{(-/-)}$ was used as loading control (Figure 6, Input). The results showed that EFhd2 was successfully immunoprecipitated from both forebrain and hindbrain of Efhd2$^{(+/+)}$ mice (Figure 6). Tagln3 and Tmod2 co-immunoprecipitated with EFhd2 from both forebrain and hindbrain of Efhd2$^{(+/+)}$ mice (Figure 6). No signal was detected in Efhd2$^{(-/-)}$ control (Figure 6). Despite similar amounts of EFhd2 detected in both regions, the intensity of Tagln3 and Tmod2 signals were higher in the forebrain than the hindbrain samples. In contrast, a similar Coro2b protein signal was detected at the expected molecular weight in both forebrain and hindbrain samples from Efhd2$^{(+/+)}$ mice (Figure 6). A cross reacting band was also detected in samples from Efhd2$^{(-/-)}$ mice, but the Coro2b signal was much higher in the Efhd2$^{(+/+)}$, suggesting that the signal could be due to cross reaction with a non-specific protein in the sample or background signal from the secondary antibody. Western blot was conducted excluding the anti-Coro2b antibody and incubating with secondary antibody alone. The results showed a protein band at the same molecular weight in the IP samples indicating that the background signal comes from the secondary antibody used (Figure 6). Myh9 and Myh10 also co-immunoprecipitated with EFhd2 in forebrain and hindbrain from Efhd2$^{(+/+)}$ mice. However, their signals were higher in the forebrain samples than the hindbrain samples. Nevertheless, these results

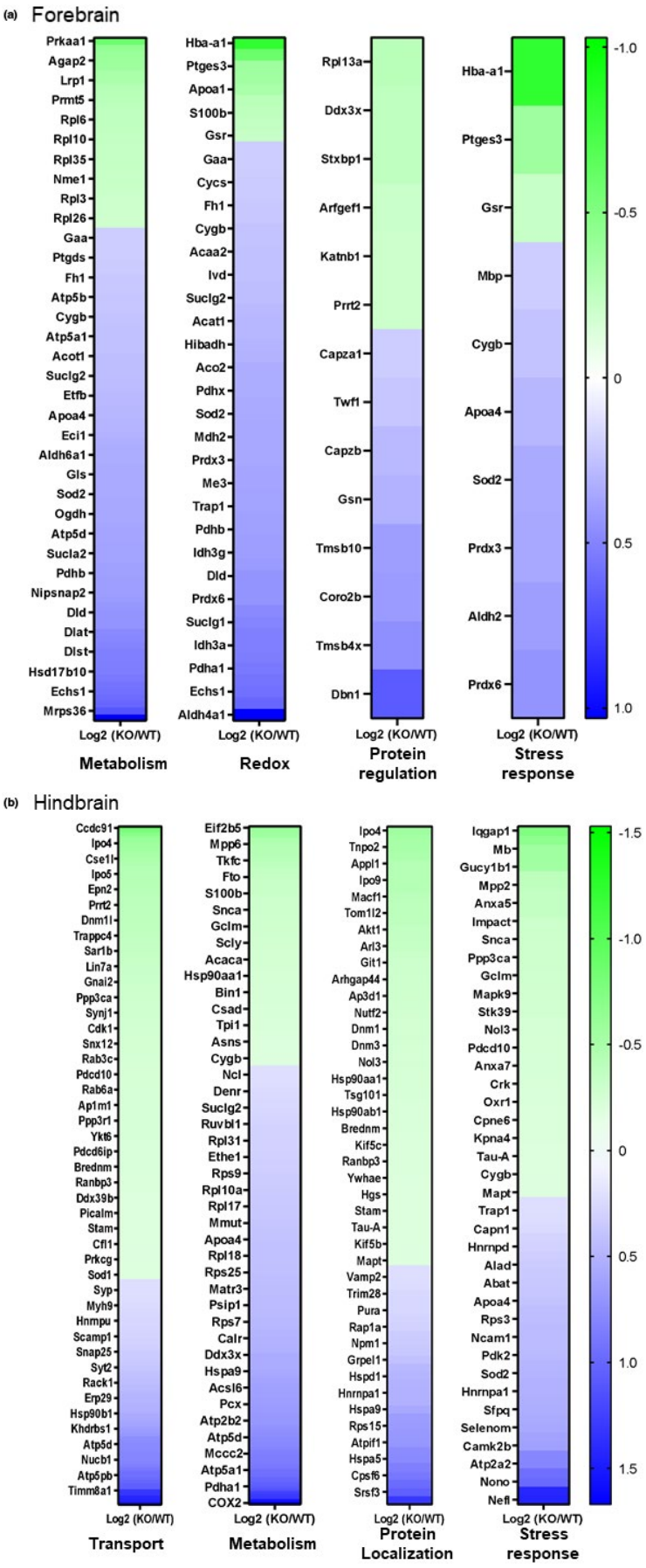

FIGURE 4 Global proteome changes upon Efhd2 deletion. Heatmaps demonstrating abundance change of proteins detected by LFQ in (a) forebrain and (b) hindbrain. Data are represented as Log2 Efhd2$^{(-/-)}$/Efhd2$^{(+/+)}$ ratio of proteins that show ≥20% change in Efhd2$^{(-/-)}$ ($n = 6$) compared to Efhd2$^{(+/+)}$ ($n = 6$). GO analysis of differentially abundant proteins was conducted using ClueGo in Cytoscape software. ClueGo parameters were >10 proteins/term and Benjamini-Hochberg were used. Kappa score threshold is set to 0.5. (n = number of animals per genotype)

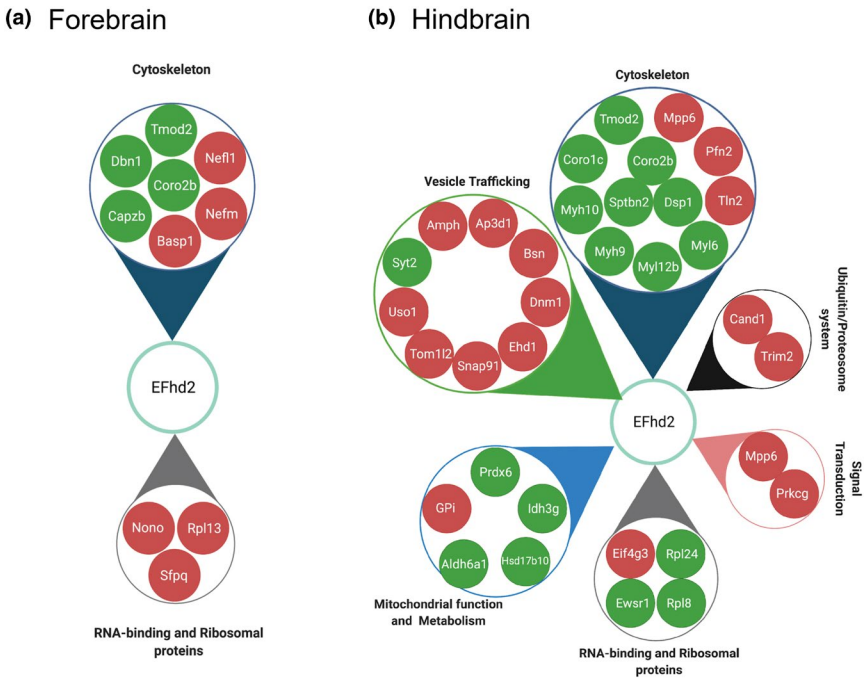

FIGURE 5 EFhd2-associated proteins with abundance change in Efhd2$^{(-/-)}$. Identified EFhd2-associated proteins were queried in the label-free quantitative proteomics data. By juxtaposing the detected proteome changes with the identified EFhd2 interactome, we found EFhd2-associated proteins with differential abundance Efhd2$^{(-/-)}$ mice ($n = 6$). (a) In the forebrain, cytoskeleton- and RNA/Ribosome-associated proteins that copurified with EFhd2 showed differential protein abundance in Efhd2$^{(-/-)}$. (b) In hindbrain regions, EFhd2-associated proteins linked to cytoskeleton, vesicle trafficking, ubiquitin/proteosome system (UPS), signal transduction, mitochondrial function, and RNA/ ribosomal binding show differential abundance in Efhd2$^{(-/-)}$. Green nodes indicate increased abundance and red nodes indicate decreased abundance. Figure created in Biorender.com. (n = number of animals per genotype)

confirm the co-immunoprecipitation of EFhd2 with known proteins that modulate actin filaments dynamics and organization.

Targeted mass spectrometry (tMS) is used to detect specific peptides ions from a protein of interest. The IP samples were digested with trypsin and subjected to tMS. To develop a PRM approach, two peptides were selected for each protein that were previously detected by MS. The total area under the curve of the detected peptide ions was calculated from both forebrain and hindbrain immunoprecipitates from Efhd2$^{(+/+)}$ and Efhd2$^{(-/-)}$. Fragmentation product ions were confronted to a mouse library that provided an independent confirmation of the expected peptide ion fragments (dot product value >0.7). First, we used tMS to validate the five proteins (Tagln3, Tmod2, Coro2b, Myh9 and Myh10) detected by western blot (Table S7). The selected peptide ions for Tagln3 and Coro2B proteins were detected only in the forebrain and hindbrain of Efhd2$^{(+/+)}$ mice (Table S7). These results are consistent with the western blot data that shows no detection of Tagln3 and Coro2B protein bands in Efhd2$^{(-/-)}$ (Figure 6). The selected peptides for Tmod2, Myh9 and Myh10 were detected in the forebrain of Efhd2$^{(+/+)}$ mice and not in Efhd2$^{(-/-)}$. Myh9 and Myh10 selected peptides were detected in the hindbrain of both Efhd2$^{(+/+)}$ and Efhd2$^{(-/-)}$. However, the level of detection for these peptide ions in the hindbrain of Efhd2$^{(+/+)}$ was 6 to 10 times higher than the detected in Efhd2$^{(-/-)}$ samples (Table S7). These findings also accord with the western blot data that shows a background signal in the Efhd2$^{(-/-)}$ samples (Figure 6). We selected peptide ions for three other proteins, namely Drebrin (Dbn1), F-actin-capping protein subunit alpha-2 (Capza2) and RNA-binding protein EWS (Ewrs1) (Table S7). The selected peptides ions for these three proteins were also detected at a higher level in both the forebrain and hindbrain of Efhd2$^{(+/+)}$ samples than Efhd2$^{(-/-)}$. These results validate the co-purification of Dbn1, Capza2 and Ewrs1 with EFhd2 proteins from both forebrain and hindbrain. Interestingly, these three proteins have been associated with AD pathophysiology (Harigaya et al., 1996; Lee et al., 2019; Vanderburg et al., 2010). Lastly, these results also demonstrate that tMS can be used for validation of novel identified associated proteins.

4 | DISCUSSION

We provide a broad molecular perspective of EFhd2 interactome in mouse brain. Previous in vitro studies demonstrated that EFhd2 is implicated in actin filament dynamics and signaling pathways as a scaffold protein. Furthermore, it has been shown that EFhd2 is associated with motor proteins in vitro. However, it is still unclear whether EFhd2 is associated with these biological functions in mouse brain tissue. Our data illustrate the association of EFhd2 with several molecular processes and provide a framework to prioritize future studies directed to elucidate EFhd2's physiological and pathological role.

Several studies have indicated that EFhd2 colocalizes with F-actin in cell protrusions and lamellipodia in vitro using various cell

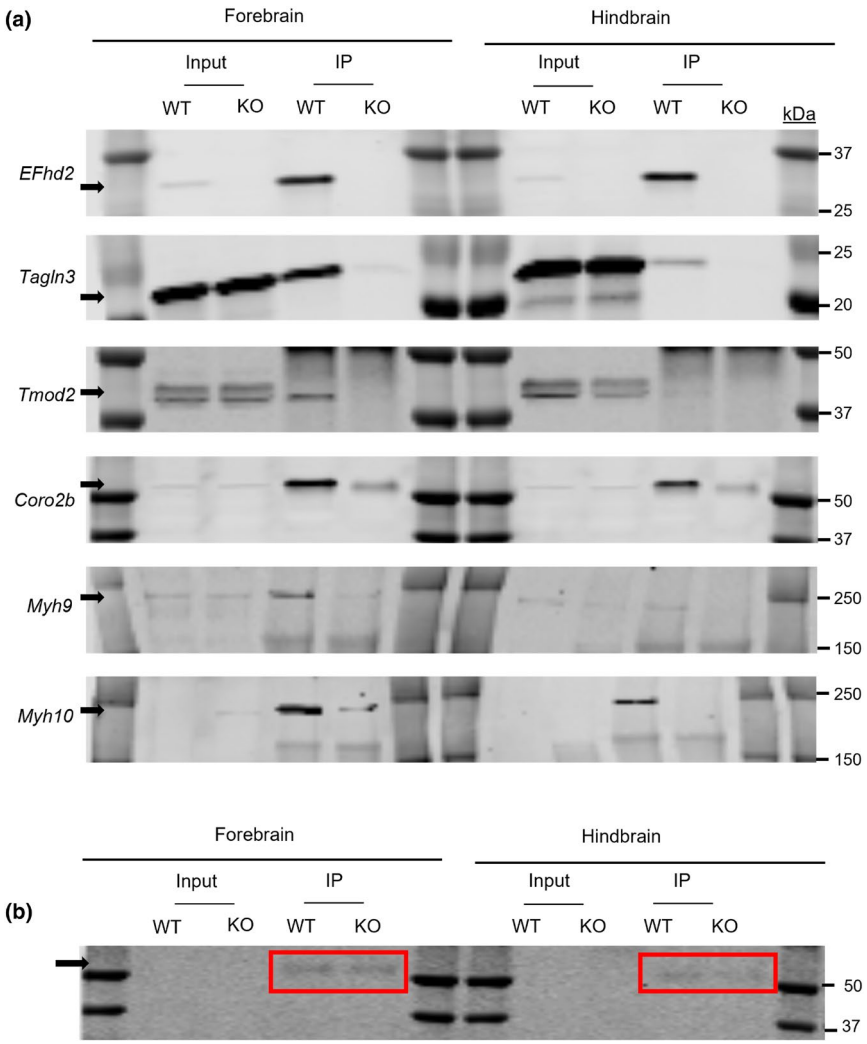

FIGURE 6 Validation of EFhd2-associated proteins. Forebrains and hindbrains from 11 to 12 months. female Efhd2$^{(+/+)}$ ($n = 3$) and Efhd2$^{(-/-)}$ ($n = 3$) were homogenized, and EFhd2 was immunoprecipitated by anti-EFhd2 (clone 10D6). (a) Western blot was conducted with anti-EFhd2 (1:5000) to verify the IP. Primary antibodies used to validate co-immunoprecipitation of selected proteins are anti-Transgelin 3 (Tagln3), anti-Tropomodulin 2 (Tmod2), anti-Coronin 2b (Coro2b), anti-Myosin 2a (Myh9), and anti-Myosin 2b (Myh10). All the selected EFhd2-associated proteins in the forebrain and hindbrain regions at the expected molecular weight (black arrow). None of them were identified in the IP from Efhd2$^{(-/-)}$. (b) Western blot conducted without primary antibody to verify the background signal observed at ~50 kDa. The signal was observed at the same molecular weight (arrow) indicating that corresponds to a secondary antibody cross-reacting band. Input is 45 μg of postnuclear brain lysate. Molecular weight marker is indicated by kDa. (n = number of animals per genotype)

models (Ramesh et al., 2009; Huh et al., 2013; Kwon et al., 2013; Park et al., 2017) Furthermore, EFhd2 overexpression induces cell spreading and lamellipodia formation whereas EFhd2 knock down inhibits cell migration (Kwon et al., 2013; Kogias et al., 2019) Moreover, EFhd2 colocalizes with tau, tubulin, and actin in the leading edge of primary neurons (Purohit et al., 2014) In cell-free assays, EFhd2 increases actin bundling and inhibits cofilin-mediated actin depolymerization (Huh et al., 2013) Here, we identified that EFhd2 is associated with several actin-binding proteins that regulate filament organization, actin polymerization and depolymerization, and cross-linking. A recent study has reported that Coro2b is predominantly expressed in the CNS and is enriched in growth cones wherein it interacts with F-actin to reduce the speed of F-actin filaments. They showed also that Coro2b is required for dendrite development and its coiled-coil domain mediates self-oligomerization, which is required to inhibit actin polymerization. We showed that EFhd2's coiled-coil domain is required for its self-oligomerization and association with tau proteins (Ferrer-Acosta, Rodríguez-Cruz, et al., 2013). Thus, it is plausible to speculate that EFhd2 promotes actin filament formation by associating with Coro2b through their coiled-coil domains, which prevents Coro2b from interacting with F-actin. Interestingly, Tmod2, another identified EFhd2-associated protein, serves as an end-actin filament cap to stabilize the filaments, preventing elongation and depolymerization, specifically at the dendrites. These findings suggest that EFhd2 role in actin filaments dynamics is through its interaction with known actin-binding proteins. Future studies should reveal molecular pathways that control the interaction between EFhd2 and actin-binding proteins in CNS. Not only is EFhd2 associated with actin-binding proteins, but it is also associated with microtubules- and intermediate filaments-regulating proteins, as well as known actin-motor proteins (e.g., Myh9 and Myh10). Collectively, EFhd2 might be a modulator of cytoskeleton dynamics and translocation.

EFhd2 decreases kinesin-mediated microtubule gliding in vitro (Purohit et al., 2014). Interestingly, numerous proteins that regulate disparate trafficking pathways copurified with EFhd2. No previous reports have shown that EFhd2 regulates vesicle trafficking. Although we cannot determine whether EFhd2 directly associates with vesicle trafficking proteins or this association is secondary to its interaction with cytoskeleton, more studies will be required to unveil this molecular aspect of EFhd2 function that has not been studied before. In particular, mouse forebrain EFhd2 was associated with Sytl4 and its physiological interactor Rab8a that together bind to SNARE complex and regulate vesicle docking and fusion

(Hampson et al., 2013). Likewise, EFhd2 in the hindbrain was associated with Amph and Dnm1 that mediate Clathrin-dependent endocytosis (Grabs et al., 1997). Based on these observations, we hypothesize that EFhd2 might act as a scaffold that recruits protein complexes needed for subsequent target interaction. This hypothesis is supported by a previous study that showed EFhd2 as a scaffold recruiting BCR, Syk, and PLCγ to regulate BCR-induced Ca^{2+} influx in WEHI-231 cells (Kroczek et al., 2010).

We also show the association of EFhd2 and signaling proteins. For instance, we identified Camk2a (αCamkII) in association with EFhd2 in mouse forebrain regions. Previous studies suggested that EFhd2 may modulate signaling pathways in response to Ca^{2+} oscillations. However, no direct association between EFhd2 and protein complexes that control synaptic function has been previously reported. The identified association between EFhd2 and αCamkII indicate that EFhd2 may exert a direct effect on proteins regulated by changes in Ca^{2+} levels that are involved in synaptic plasticity. Both EFhd2 and αCamkII play a role in controlling addiction behavior. αCamkII autophosphorylation at T286 mediates the autonomous αCamkII activity independent of Ca^{2+}/calmodulin (Glazewski et al., 2000). Autophosphorylated αCamkII is important for inducing long-term potentiation in neocortical experience-dependent plasticity. The autonomous activity of αCamkII due to autophosphorylation amplifies Ca^{2+} signaling, and it is linked to drug seeking behavior (Anderson et al., 2008; Easton et al., 2013). Consistently, the expression of αCamkII autophosphorylation mutant (T286A) reduces alcohol consumption in mice and attenuates initial alcohol preference (Easton et al., 2013). Expression of αCamkII mutant (T286A) also led to no detectable dopamine increase upon alcohol challenge (Easton et al., 2013). In another study, the inhibition of αCamkII in the ventral tegmental area (VTA) affected cocaine-evoked synaptic plasticity, suggesting that αCamkII activity is required for cocaine conditioning (Anderson et al., 2008). In contrast, it was shown that $Efhd2^{(-/-)}$ mice consume more alcohol than wild-type mice and develop an increased sensation-seeking behavior and low anxiety (Mielenz et al., 2018). Interestingly, deletion of Efhd2 lead to enhanced excitability of dopaminergic neurons in VTA and enhanced extracellular dopamine response upon treatment with psychostimulant drugs (Kogias et al., 2019; Mielenz et al., 2018). These results suggest that EFhd2 may modulate synaptic activity to prevent the development of addictions. Moreover, a SNP (rs112146896) in EFHD2 gene was positively associated with high frequency of alcohol consumption in an adolescent population (European School Survey Project). Taken together, EFhd2 might be a negative modulator of autonomous αCamkII activity, rendering EFhd2 protective against addiction. Further studies are required to determine whether EFhd2 directly interacts with autophosphorylated αCamkII and, hence, inhibits αCamkII activity. Additionally, future experiments should unravel whether the interaction between EFhd2 and αCamkII is Ca^{2+} dependent.

We identified molecular associations with EFhd2 in forebrain and hindbrain regions that have yet to be examined. Particularly, molecular chaperones and UPS components co-immunoprecipitated with EFhd2. These proteins regulate stress response by maintaining proper protein folding, preventing abnormal aggregation, and degrading misfolded proteins. Moreover, several mitochondrial chaperones that mediate mitochondrial homeostasis were also identified. UPS and chaperones machinery are regulated by different signaling pathways. In this regard, signal transduction proteins known to modulate the UPS system, such as ERK1 and 14-3-3 proteins, also co-immunoprecipitated with EFhd2. These signal transduction proteins govern downstream signaling cascades pivotal for cell survival, neuronal growth, and axonal transport. Moreover, EFhd2 is associated with ribosomal and RNA-binding proteins involved in regulating translation and transcription efficiency. These unprecedented molecular associations of EFhd2 merit further investigation to validate the possible role of EFhd2 in controlling protein expression and degradation.

To gain further insights into EFhd2's physiological function, we evaluated the global proteome changes in forebrain and hindbrain brain regions of $Efhd2^{(-/-)}$ compared to $Efhd2^{(+/+)}$ using LFQ mass spectrometry. By grouping the differentially abundant proteins, we found that mainly metabolic, stress response, redox response, and protein regulation showed abundance changes upon deletion of Efhd2 gene in the forebrain. In the hindbrain, the biological functions mainly represented of the differential abundant proteins in $Efhd2^{(-/-)}$ are metabolism, stress response, protein localization, and transport. We also show that the abundance of several identified EFhd2-associated proteins also changed upon Efhd2 gene deletion (Figure 5 and Tables S5 and S6). These data suggest that the identified changes could be compensatory mechanisms to mitigate the consequences of Efhd2 gene deletion. This could explain, in part, the fact that we and others did not observe developmental or morphological anomalies in $Efhd2^{(-/-)}$ (Purohit et al., 2014; Rodriguez-Cruz, 2014). Indeed, these data raise few questions: Do the observed protein changes denote a compensatory mechanism for cytoskeleton and vesicle trafficking? What are the pathological ramifications of EFhd2 dysregulation? These questions and others are worth examining to better understand the physiological role of EFhd2 in the brain and its role in neurological disorders.

Several limitations of our data analysis are worth noting. Quantitation after IP was not done due to the technical variability in this approach. To account for sample and technical variability, we grouped biological replicates (e.g., IPs from the same brain region). The rigorous experimental design and stringent data curation criteria used to identify EFhd2-associated proteins may have excluded bona fide EFhd2-associated proteins that tend to bind non-specifically to beads. For example, we could not list actin among the curated EFhd2-associated proteins in mouse since it was detected among proteins identified in the negative controls. In addition, we noticed that the number of detected EFhd2-associated proteins is variable among different regions of mice brains. This variability can be ascribed to the limited efficiency of IP to capture some protein–protein interactions. Nevertheless, we validated several proteins identified as EFhd2-associated proteins using western blot and tMS. On the other hand, conducting GO of differentially abundant proteins using ClueGo imposes a limitation in data analysis by setting threshold of >10 proteins/term. Therefore, not all the detected proteins were

included, which could overlook other biological functions that may be impacted by the deletion of Efhd2. For this reason, we used literature searches to group EFhd2-associated proteins into their biological functions. Finally, even though we report all proteins detected by LFQ, we set a threshold at log2 ±0.2 (20%) to be included in our data analysis, based on expected variations due to median protein half-life. However, proteins that showed less than 20% change, not related to their natural rate of turn over, may also be biologically relevant.

Validating MS proteomics data has specific challenges that need to be acknowledged. The first challenge is the selection of proteins to be validated. Here, the identification of EFhd2-associated proteins depends on differential interaction given the variable regulation of biological mechanisms needed for these associations. Based on this expected variability, we established a stepwise selection process for validating EFhd2-associated proteins (see Methods). The second challenge is comparing results from two techniques with different sensitivity levels. Western blot depends on the use of antibodies with different binding constants and specificity to their respective antigen. Therefore, variability in the detection sensitivity of the antibodies render them inefficient regardless of their specificity to the targeted protein. Accordingly, we developed a tMS approach. tMS detects specific ions taking in consideration an established targeting criteria based on mass, charge state, and retention time. This method has both the sensitivity and specificity required to validate the identified EFhd2-associated proteins. The third challenge is determining direct versus indirect interaction. Despite the identified EFhd2-associated proteins, we cannot conclude that these proteins interact directly with EFhd2 or deduce clear molecular implications of the identified associations. Nevertheless, our findings uncovered novel EFhd2-associated proteins that delineate the mouse EFhd2 brain interactome, providing the groundwork to further characterize the physiological role of EFhd2 in regulating inextricable cellular processes and molecular pathways.

ACKNOWLEDGMENTS

The authors acknowledge Dr Jack Lipton's support and the Department of Translational Neuroscience for providing financial support to complete this study. The NIH Grant No. P30AG053760 supports part of this study.

All experiments were conducted in compliance with the ARRIVE guidelines.

AUTHOR CONTRIBUTION STATEMENT

I.E.V. conceived the project and designed experiments; A.S.S., A.U., T. G., N.M.K., A.L., J.R. and J.L. performed and/or interpreted experiments; I.E.V. and A.S.S. wrote the manuscript and all other authors proofread and edited.

CONFLICT OF INTEREST

The authors declare no conflict of interest.

DATA AVAILABILITY STATEMENT

Data are included in the article Supplementary material and available on request from the authors.

ORCID

Ahlam S. Soliman https://orcid.org/0000-0001-5157-7932
Nicholas M. Kanaan https://orcid.org/0000-0002-4362-2593
Irving E. Vega https://orcid.org/0000-0002-7960-9534

REFERENCES

Anderson, S. M., Famous, K. R., Sadri-Vakili, G., Kumaresan, V., Schmidt, H. D., Bass, C. E., Terwilliger, E. F., Cha, J.-H.- J., & Pierce, R. C. (2008). CaMKII: A biochemical bridge linking accumbens dopamine and glutamate systems in cocaine seeking. *Nature Neuroscience*, 11, 344–353. https://doi.org/10.1038/nn2054.

Avramidou, A., Kroczek, C., Lang, C., Schuh, W., Jäck, H., & Mielenz, D. (2007). The novel adaptor protein Swiprosin-1 enhances BCR signals and contributes to BCR-induced apoptosis. *Cell Death & Differentiation*, 14, 1936–1947. https://doi.org/10.1038/sj.cdd.4402206.

Binder, L. I., Frankfurter, A., & Rebhun, L. I. (1985). The distribution of tau in the mammalian central nervous system. *Journal of Cell Biology*, 101, 1371–1378. https://doi.org/10.1083/jcb.101.4.1371.

Borger, E., Herrmann, A., Mann, D. A., Spires-Jones, T., & Gunn-Moore, F. (2014). The calcium-binding protein EFhd2 modulates synapse formation in vitro and is linked to human dementia. *Journal of Neuropathology & Experimental Neurology*, 73, 1166–1182. https://doi.org/10.1097/NEN.0000000000000138.

Brunger, A. T., Weninger, K., Bowen, M., & Chu, S. (2009). Single-molecule studies of the neuronal SNARE fusion machinery. *Annual Review of Biochemistry*, 78, 903–928. https://doi.org/10.1146/annurev.biochem.77.070306.103621.

Cajigas, I. J., Tushev, G., Will, T. J., tom Dieck, S., Fuerst, N., & Schuman, E. M. (2012). The local transcriptome in the synaptic neuropil revealed by deep sequencing and high-resolution imaging. *Neuron*, 74, 453–466. https://doi.org/10.1016/j.neuron.2012.02.036.

Cao, X., Ballew, N., & Barlowe, C. (1998). Initial docking of ER-derived vesicles requires Uso1p and Ypt1p but is independent of SNARE proteins. *The EMBO Journal*, 17, 2156–2165. https://doi.org/10.1093/emboj/17.8.2156.

CHEMDATA.NIST.GOV (2021) Libraries of Peptide Tandem Mass Spectra.

Drasbek, K. R., Holm, M. M., Delenclos, M., & Jensen, K. (2008). Mapping of the spontaneous deletion in the Ap3d1 gene of mocha mice: fast and reliable genotyping. *BMC Research Notes*, 1, 1–7. https://doi.org/10.1186/1756-0500-1-119.

Dujardin, S., Bégard, S., Caillierez, R., Lachaud, C., Carrier, S., Lieger, S., Gonzalez, J. A., Deramecourt, V., Déglon, N., Maurage, C.-A., Frosch, M. P., Hyman, B. T., Colin, M., & Buée, L. (2018). Different tau species lead to heterogeneous tau pathology propagation and misfolding. *Acta Neuropathologica Communications*, 6, 1–12. https://doi.org/10.1186/s40478-018-0637-7.

Easton, A. C., Lucchesi, W., Lourdusamy, A., Lenz, B., Solati, J., Golub, Y., Lewczuk, P., Fernandes, C., Desrivieres, S., Dawirs, R. R., Moll, G. H., Kornhuber, J., Frank, J., Hoffmann, P., Soyka, M., Kiefer, F., Schumann, G., Peter Giese, K., & Müller, C. P. (2013). α CaMKII autophosphorylation controls the establishment of alcohol drinking behavior. *Neuropsychopharmacology*, 38, 1636–1647. https://doi.org/10.1038/npp.2013.60.

Farías, G. G., Guardia, C. M., De Pace, R., Britt, D. J., & Bonifacino, J. S. (2017). BORC/kinesin-1 ensemble drives polarized transport of lysosomes into the axon. *Proceedings of the National Academy of Sciences*, 114, E2955–E2964. https://doi.org/10.1073/pnas.1616363114.

Ferrer-Acosta, Y., Rodríguez Cruz, E. N., Vaquer, A. D. C., & Vega, I. E. (2013). Functional and structural analysis of the conserved EFhd2 protein. *Protein and Peptide Letters*, 20, 573–583.

Ferrer-Acosta, Y., Rodríguez-Cruz, E. N., Orange, F., De Jesús-Cortés, H., Madera, B., Vaquer-Alicea, J., Ballester, J., Guinel, M.-F., Bloom, G. S., & Vega, I. E. (2013). EFhd2 is a novel amyloid protein

associated with pathological tau in Alzheimer's disease. *Journal of Neurochemistry*, 125, 921–931. https://doi.org/10.1111/jnc.12155.

Ferrer-Orta, C., Perez-Sanchez, M. D., Coronado-Parra, T., Silva, C., Lopez-Martinez, D., Baltanas-Copado, J., Gomez-Fernandez, J. C., Corbalan-Garcia, S., & Verdaguer, N. (2017). Structural characterization of the Rabphilin-3A-SNAP25 interaction. *Proceedings of the National Academy of Sciences USA*, 114, E5343–E5351. https://doi.org/10.1073/pnas.1702542114.

Fukuda, Y., Pazyra-Murphy, M. F., Silagi, E. S., Tasdemir-Yilmaz, O. E., Li, Y., Rose, L., Yeoh, Z. C., Vangos, N. E., Geffken, E. A., Seo, H.-S., Adelmant, G., Bird, G. H., Walensky, L. D., Marto, J. A., Dhe-Paganon, S., & Segal, R. A. (2021). Binding and transport of SFPQ-RNA granules by KIF5A/KLC1 motors promotes axon survival. *Journal of Cell Biology*, 220(1), e202005051. http://dx.doi.org/10.1083/jcb.202005051.

Gaertner, T. R., Kolodziej, S. J., Wang, D., Kobayashi, R., Koomen, J. M., Stoops, J. K., & Waxham, M. N. (2004). Comparative analyses of the three-dimensional structures and enzymatic properties of α, β, γ, and δ isoforms of Ca2+-calmodulin-dependent protein kinase II. *Journal of Biological Chemistry*, 279, 12484–12494. https://doi.org/10.1074/jbc.M313597200.

Glazewski, S., Giese, K., Silva, A., & Fox, K. (2000). The role of α-CaMKII autophosphorylation in neocortical experience-dependent plasticity. *Nature Neuroscience*, 3, 911–918. https://doi.org/10.1038/78820.

Gong, B., Radulovic, M., Figueiredo-Pereira, M. E., & Cardozo, C. (2016). The ubiquitin-proteasome system: Potential therapeutic targets for Alzheimer's disease and spinal cord injury. *Frontiers in Molecular Neuroscience*, 9, 4. https://doi.org/10.3389/fnmol.2016.00004.

Götz, J., Halliday, G., & Nisbet, R. M. (2019). Molecular pathogenesis of the tauopathies. *Annual Review of Pathology: Mechanisms of Disease*, 14, 239–261. https://doi.org/10.1146/annurev-pathmechdis-012418-012936.

Grabinski, T., & Kanaan, N. M. (2016). Novel non-phosphorylated serine 9/21 GSK3β/α antibodies: Expanding the tools for studying GSK3 regulation. *Frontiers in Molecular Neuroscience*, 9, 123. https://doi.org/10.3389/fnmol.2016.00123.

Grabs, D., Slepnev, V. I., Songyang, Z., David, C., Lynch, M., Cantley, L. C., & De Camilli, P. (1997). The SH3 domain of amphiphysin binds the proline-rich domain of dynamin at a single site that defines a new SH3 binding consensus sequence. *Journal of Biological Chemistry*, 272, 13419–13425. https://doi.org/10.1074/jbc.272.20.13419.

Hampson, A., O'Connor, A., & Smolenski, A. (2013). Synaptotagmin-like protein 4 and Rab8 interact and increase dense granule release in platelets. *Journal of Thrombosis and Haemostasis*, 11, 161–168.

Harigaya, Y., Shoji, M., Shirao, T., & Hirai, S. (1996). Disappearance of actin-binding protein, drebrin, from hippocampal synapses in Alzheimer's disease. *Journal of Neuroscience Research*, 43, 87–92. https://doi.org/10.1002/jnr.490430111.

Huh, Y. H., Kim, S. H., Chung, K.-H., Oh, S., Kwon, M.-S., Choi, H.-W., Rhee, S., Ryu, J.-H., Park, Z. Y., Jun, C.-D., & Song, W. K. (2013). Swiprosin-1 modulates actin dynamics by regulating the F-actin accessibility to cofilin. *Cellular and Molecular Life Sciences*, 70, 4841–4854. https://doi.org/10.1007/s00018-013-1447-5.

Huh, Y. H., Oh, S., Yeo, Y. R., Chae, I. H., Kim, S. H., Lee, J. S., Yun, S. J., Choi, K. Y., Ryu, J.-H., Jun, C.-D., & Song, W. K. (2015). Swiprosin-1 stimulates cancer invasion and metastasis by increasing the Rho family of GTPase signaling. *Oncotarget*, 6, 13060. https://doi.org/10.18632/oncotarget.3637.

Jahn, R., & Fasshauer, D. (2012). Molecular machines governing exocytosis of synaptic vesicles. *Nature*, 490, 201–207. https://doi.org/10.1038/nature11320.

Kamerkar, S. C., Kraus, F., Sharpe, A. J., Pucadyil, T. J., & Ryan, M. T. (2018). Dynamin-related protein 1 has membrane constricting and severing abilities sufficient for mitochondrial and peroxisomal fission. *Nature Communications*, 9, 1–15. https://doi.org/10.1038/s41467-018-07543-w.

Kanai, Y., Dohmae, N., & Hirokawa, N. (2004). Kinesin transports RNA: Isolation and characterization of an RNA-transporting granule. *Neuron*, 43, 513–525. https://doi.org/10.1016/j.neuron.2004.07.022.

Khazaei, M. R., Bunk, E. C., Hillje, A. L., Jahn, H. M., Riegler, E. M., Knoblich, J. A., Young, P., & Schwamborn, J. C. (2011). The E3-ubiquitin ligase TRIM2 regulates neuronal polarization. *Journal of Neurochemistry*, 117, 29–37. https://doi.org/10.1111/j.1471-4159.2010.06971.x.

Kitao, Y., Hashimoto, K., Matsuyama, T., Iso, H., Tamatani, T., Hori, O., Stern, D.M., Kano, M., Ozawa, K., & Ogawa, S. (2004). ORP150/HSP12A regulates Purkinje cell survival: A role for endoplasmic reticulum stress in cerebellar development. *Journal of Neuroscience*, 24(6), 1486–1496. http://dx.doi.org/10.1523/jneurosci.4029-03.2004.

Kogias, G., Kornhuber, J., Reimer, D., Mielenz, D., & Muller, C. P. (2019). Swiprosin-1/ EFhd2: From immune regulator to personality and brain disorders. *Neurosignals*, 27, 1–19.

Kogias, G., Zheng, F., Kalinichenko, L. S., Kornhuber, J., Alzheimer, C., Mielenz, D., & Muller, C. P. (2020). Swiprosin1/EFhd2 is involved in the monoaminergic and locomotor responses of psychostimulant drugs. *Journal of Neurochemistry*, 154, 424–440. https://doi.org/10.1111/jnc.14959.

Kroczek, C., Lang, C., Brachs, S., Grohmann, M., Dütting, S., Schweizer, A., Nitschke, L., Feller, S. M., Jäck, H.-M., & Mielenz, D. (2010). Swiprosin-1/EFhd2 controls B cell receptor signaling through the assembly of the B cell receptor, Syk, and phospholipase C γ2 in membrane rafts. *The Journal of Immunology*, 184, 3665–3676. https://doi.org/10.4049/jimmunol.0903642.

Kwon, M.-S., Park, K. R., Kim, Y.-D., Na, B.-R., Kim, H.-R., Choi, H.-J., Piragyte, I., Jeon, H., Chung, K. H., Song, W. K., Eom, S. H., & Jun, C.-D. (2013). Swiprosin-1 Is a novel actin bundling protein that regulates cell spreading and migration. *PLoS ONE*, 8(8), e71626. http://dx.doi.org/10.1371/journal.pone.0071626.

Lee, J., Nguyen, P. T., Shim, H. S., Hyeon, S. J., Im, H., Choi, M.-H., Chung, S., Kowall, N. W., Lee, S. B., & Ryu, H. (2019). EWSR1, a multifunctional protein, regulates cellular function and aging via genetic and epigenetic pathways. *Biochimica et Biophysica Acta (BBA) - Molecular Basis of Disease*, 1865(7), 1938–1945. http://dx.doi.org/10.1016/j.bbadis.2018.10.042.

Lesage, S., Drouet, V., Majounie, E., Deramecourt, V., Jacoupy, M., Nicolas, A., Cormier-Dequaire, F., Hassoun, S. M., Pujol, C., Ciura, S., Erpapazoglou, Z., Usenko, T., Maurage, C.-A., Sahbatou, M., Liebau, S., Ding, J., Bilgic, B., Emre, M., Erginel-Unaltuna, N., … Brice, A. (2016). Loss of VPS13C function in autosomal-recessive parkinsonism causes mitochondrial dysfunction and increases PINK1/Parkin-dependent mitophagy. *American Journal of Human Genetics*, 98, 500–513. https://doi.org/10.1016/j.ajhg.2016.01.014.

Levin, Y. (2011). The role of statistical power analysis in quantitative proteomics. *Proteomics*, 11, 2565–2567. https://doi.org/10.1002/pmic.201100033.

Meng, J.-J., Bornslaeger, E. A., Green, K. J., Steinert, P. M., & Ip, W. (1997). Two-hybrid analysis reveals fundamental differences in direct interactions between desmoplakin and cell type-specific intermediate filaments. *Journal of Biological Chemistry*, 272, 21495–21503. https://doi.org/10.1074/jbc.272.34.21495.

Mielenz, D., Reichel, M., Jia, T., Quinlan, E. B., Stöckl, T., Mettang, M., Zilske, D., Kirmizi-Alsan, E., Schönberger, P., Praetner, M., Huber, S. E., Amato, D., Schwarz, M., Purohit, P., Brachs, S., Spranger, J., Hess, A., Büttner, C., Ekici, A. B., … Müller, C. P. (2018). EFhd2/Swiprosin-1 is a common genetic determinator for sensation-seeking/low anxiety and alcohol addiction. *Molecular Psychiatry*, 23, 1303–1319. https://doi.org/10.1038/mp.2017.63.

Park, K. R., An, J. Y., Kang, J. Y., Lee, J.-G., Lee, Y., Mun, S. A., Jun, C.-D., Song, W. K., & Eom, S. H. (2017). Structural mechanism underlying regulation of human EFhd2/Swiprosin-1 actin-bundling activity by Ser183 phosphorylation. *Biochemical and Biophysical Research*

Communications, 483, 442–448. https://doi.org/10.1016/j.bbrc.2016.12.124.

Peled, M., Dragovich, M. A., Adam, K., Strazza, M., Tocheva, A. S., Vega, I. E., & Mor, A. (2018). EF hand domain family member D2 is required for T cell cytotoxicity. *The Journal of Immunology*, 201, 2824–2831. https://doi.org/10.4049/jimmunol.1800839.

Pettitt, S. J., Liang, Q., Rairdan, X. Y., Moran, J. L., Prosser, H. M., Beier, D. R., Lloyd, K. C., Bradley, A., & Skarnes, W. C. (2009). Agouti C57BL/6N embryonic stem cells for mouse genetic resources. *Nature Methods*, 6, 493–495. https://doi.org/10.1038/nmeth.1342.

Pierce, N. W., Lee, J. E., Liu, X., Sweredoski, M. J., Graham, R. L. J., Larimore, E. A., Rome, M., Zheng, N., Clurman, B. E., Hess, S., Shan, S.-O., & Deshaies, R. J. (2013). Cand1 promotes assembly of new SCF complexes through dynamic exchange of F box proteins. *Cell*, 153, 206–215. https://doi.org/10.1016/j.cell.2013.02.024.

Power, J. H., Asad, S., Chataway, T. K., Chegini, F., Manavis, J., Temlett, J. A., Jensen, P. H., Blumbergs, P. C., & Gai, W.-P. (2008). Peroxiredoxin 6 in human brain: Molecular forms, cellular distribution and association with Alzheimer's disease pathology. *Acta Neuropathologica*, 115, 611–622. https://doi.org/10.1007/s00401-008-0373-3.

Pratt, W., Morishima, Y., Murphy, M., & Harrell, M. (2006). Chaperoning of glucocorticoid receptors. *Molecular Chaperones in Health and Disease*, 111–138.

Purohit, P., Perez-Branguli, F., Prots, I., Borger, E., Gunn-Moore, F., Welzel, O., Loy, K., Wenzel, E. M., Grömer, T. W., Brachs, S., Holzer, M., Buslei, R., Fritsch, K., Regensburger, M., Böhm, K. J., Winner, B., & Mielenz, D. (2014). The Ca2+ sensor protein swiprosin-1/EFhd2 is present in neurites and involved in kinesin-mediated transport in neurons. *PLoS One*, 9, e103976. https://doi.org/10.1371/journal.pone.0103976.

Ramesh, T., Kim, Y.-D., Kwon, M.-S., Jun, C.-D., & Kim, S.-W. (2009). Swiprosin-1 regulates cytokine expression of human mast cell line HMC-1 through actin remodeling. *Immune Network*, 9, 274–284. https://doi.org/10.4110/in.2009.9.6.274.

Regensburger, M., Prots, I., Reimer, D., Brachs, S., Loskarn, S., Lie, D. C., Mielenz, D., & Winner, B. (2018). Impact of swiprosin-1/Efhd2 on adult hippocampal neurogenesis. *Stem Cell Reports*, 10, 347–355. https://doi.org/10.1016/j.stemcr.2017.12.010.

Rodriguez-Cruz, E. N. (2014). Generation and Characterization on an Efhd2 Knockout Mice University of Puerto Rico, San Juan, Puerto Rico.

Söllner, T., Whiteheart, S. W., Brunner, M., Erdjument-Bromage, H., Geromanos, S., Tempst, P., & Rothman, J. E. (1993). SNAP receptors implicated in vesicle targeting and fusion. *Nature*, 362, 318–324. https://doi.org/10.1038/362318a0.

Südhof, T. C., & Rothman, J. E. (2009). Membrane fusion: Grappling with SNARE and SM proteins. *Science*, 323, 474–477. https://doi.org/10.1126/science.1161748.

Takei, K., Slepnev, V. I., Haucke, V., & De Camilli, P. (1999). Functional partnership between amphiphysin and dynamin in clathrin-mediated endocytosis. *Nature Cell Biology*, 1, 33–39. https://doi.org/10.1038/9004.

Valenzuela, D. M., Murphy, A. J., Frendewey, D., Gale, N. W., Economides, A. N., Auerbach, W., Poueymirou, W. T., Adams, N. C., Rojas, J., Yasenchak, J., Chernomorsky, R., Boucher, M., Elsasser, A. L., Esau, L., Zheng, J., Griffiths, J. A., Wang, X., Su, H., Xue, Y., … Yancopoulos, G. D. (2003). High-throughput engineering of the mouse genome coupled with high-resolution expression analysis. *Nature Biotechnology*, 21, 652–659. https://doi.org/10.1038/nbt822.

Vanderburg, C., Davis, D., Diamond, R., Kao, P., & Delalle, I. (2010). Capzb2 protein expression in the brains of patients diagnosed with Alzheimer's disease and Huntington's disease. *Translational Neuroscience*, 1, 55–58. https://doi.org/10.2478/v10134-010-0008-9.

Vazquez-Rosa, E., Rodriguez-Cruz, E. N., Serrano, S., Rodriguez-Laureano, L., & Vega, I. E. (2014). Cdk5 phosphorylation of EFhd2 at S74 affects its calcium binding activity. *Protein Science*, 23, 1197–1207. https://doi.org/10.1002/pro.2499.

Vega, I. E. (2016). EFhd2, a protein linked to Alzheimer's disease and other neurological disorders. *Frontiers in Neuroscience*, 10, 150. https://doi.org/10.3389/fnins.2016.00150.

Vega, I. E., Sutter, A., Parks, L., Umstead, A., & Ivanova, M. I. (2018). Tau's three-repeat domain and EFhd2 co-incubation leads to increased thioflavin signal. *Frontiers in Neuroscience*, 12, 879. https://doi.org/10.3389/fnins.2018.00879.

Vega, I. E., Traverso, E. E., Ferrer-Acosta, Y., Matos, E., Colon, M., Gonzalez, J., Dickson, D., Hutton, M., Lewis, J., & Yen, S. H. (2008). A novel calcium-binding protein is associated with tau proteins in tauopathy. *Journal of Neurochemistry*, 106, 96–106. https://doi.org/10.1111/j.1471-4159.2008.05339.x.

Vega, I. E., Umstead, A., & Kanaan, N. M. (2019). EFhd2 affects tau liquid-liquid phase separation. *Frontiers in Neuroscience*, 13, 845. https://doi.org/10.3389/fnins.2019.00845.

Vicente-Manzanares, M., Ma, X., Adelstein, R. S., & Horwitz, A. R. (2009). Non-muscle myosin II takes centre stage in cell adhesion and migration. *Nature Reviews Molecular Cell Biology*, 10, 778–790. https://doi.org/10.1038/nrm2786.

Wang, T., Liu, N. S., Seet, L. F., & Hong, W. (2010). The emerging role of VHS domain-containing Tom1, Tom1L1 and Tom1L2 in membrane trafficking. *Traffic*, 11, 1119–1128. https://doi.org/10.1111/j.1600-0854.2010.01098.x.

Wani, W. Y., Chatham, J. C., Darley-Usmar, V., McMahon, L. L., & Zhang, J. (2017). O-GlcNAcylation and neurodegeneration. *Brain Research Bulletin*, 133, 80–87. https://doi.org/10.1016/j.brainresbull.2016.08.002.

Wei, S., Xu, Y., Shi, H., Wong, S.-H., Han, W., Talbot, K., Hong, W., & Ong, W.-Y. (2010). EHD1 is a synaptic protein that modulates exocytosis through binding to snapin. *Molecular and Cellular Neuroscience*, 45, 418–429. https://doi.org/10.1016/j.mcn.2010.07.014.

Wynn, R. M., Davie, J. R., Cox, R. P., & Chuang, D. T. (1994). Molecular chaperones: Heat-shock proteins, foldases, and matchmakers. *The Journal of Laboratory and Clinical Medicine*, 124, 31–36.

Zhu, X., Lee, H.-G., Raina, A. K., Perry, G., & Smith, M. A. (2002). The role of mitogen-activated protein kinase pathways in Alzheimer's disease. *Neurosignals*, 11, 270–281. https://doi.org/10.1159/000067426.

Zhu, X., Sun, Z., Lee, H.-G., Siedlak, S. L., Perry, G., & Smith, M. A. (2003). Distribution, levels, and activation of MEK1 in Alzheimer's disease. *Journal of Neurochemistry*, 86, 136–142. https://doi.org/10.1046/j.1471-4159.2003.01820.x.

SUPPORTING INFORMATION

Additional supporting information may be found in the online version of the article at the publisher's website.

How to cite this article: Soliman, A. S., Umstead, A., Grabinski, T., Kanaan, N. M., Lee, A., Ryan, J., Lamp, J., & Vega, I. E. (2021). EFhd2 brain interactome reveals its association with different cellular and molecular processes. *Journal of Neurochemistry*, 159, 992–1007. https://doi.org/10.1111/jnc.15517